On Circuit-Based Hybrid Quantum Neural Networks for Remote Sensing Imagery Classification

Alessandro Sebastianelli, *Student Member, IEEE*, Daniela Alessandra Zaidenberg, *Student Member, IEEE*, Dario Spiller, *Member, IEEE*, Bertrand Le Saux, *Member, IEEE*, and Silvia Liberata Ullo, *Senior Member, IEEE*

***Abstract*—This article aims to investigate how circuit-based hybrid quantum convolutional neural networks (QCNNs) can be successfully employed as image classifiers in the context of remote sensing. The hybrid QCNNs enrich the classical architecture of convolutional neural networks by introducing a quantum layer within a standard neural network. The novel QCNN proposed in this work is applied to the land-use and land-cover classification, chosen as an Earth observation (EO) use case, and tested on the EuroSAT dataset used as the reference benchmark. The results of the multiclass classification prove the effectiveness of the presented approach by demonstrating that the QCNN performances are higher than the classical counterparts. Moreover, investigation of various quantum circuits shows that the ones exploiting quantum entanglement achieve the best classification scores. This study underlines the potentialities of applying quantum computing to an EO case study and provides the theoretical and experimental background for future investigations.**

***Index Terms*—Earth observation (EO), image classification, land-use and land-cover (LULC) classification, machine learning (ML), quantum computing (QC), quantum machine learning (QML), remote sensing.**

I. Introduction

EARTH observation (EO) has consistently leveraged technological and computational advances helping in developing novel techniques to characterize and model the human environment [1]–[3]. Given that many remote sensing missions are currently operative, carrying on board multispectral, hyperspectral, and radar sensors, and the improved capabilities in transmitting and saving a continuously increasing number of images, nowadays estimated in over 150 terabytes per day [4], the amount of data from EO applications have reached impressive volumes so that they are referred to as Big Data. At the same time, advances in computational technologies and analysis methodologies have also progressed to accommodate larger and higher resolution datasets. Image classification techniques are constantly being improved to keep up with the ever expanding stream of Big Data, and as a consequence, artificial intelligence (AI) techniques are becoming increasingly necessary tools [5], [6].

Given the need to help expand the processing techniques to deal with these high-resolution Big Data, EO is now looking toward new and innovative computation technologies [7]. This is where quantum computing (QC) will play a fundamental role [8]. Today, there is a number of differing quantum devices, such as programmable superconducting processors [9], quantum annealers [10], and photonic quantum computers [11]. However, QC still presents some technological limitations, as reported in [12] with a special concern with noise and limited error correction. Specific algorithms, namely, the noisy intermediate-scale quantum (NISQ) computing algorithms, have been designed to tackle these issues [13].

Quantum computers promise to efficiently solve important problems that are intractable on a conventional computer. For instance, in quantum systems, due to the exponentially growing physical dimensions, finding the eigenvalues of certain operators is one such intractable problem, which can be solved by combining a highly reconfigurable photonic quantum processor with a conventional computer [14], [15].

Another example is the case of the variational quantum eigensolver (VQE) algorithm used to solve combinatorial optimization problems such as finding the ground state energy of a molecule. The algorithm finds a bound to the lowest eigenenergy of a given Hamiltonian [15]. This is, in essence, a kind of cost function, which is defined by the expectation of the molecular Hamiltonian of a given prepared eigenstate. The goal of the VQE is to minimize this cost function by varying the parameters θ used to prepare the ansatz eigenstate often representative of a molecule. This hybrid algorithm prepares and determines eigenenergies through quantum circuits, and then, it varies the parameter classically. By iterating through these classical variations and quantum calculations, a hybrid minimization process is established [14]. This approximation of critical minima is analogous to the gradient descent.

In QC, a qubit or quantum bit is the basic unit of quantum information, i.e., the quantum version of the classic binary bit. A qubit is one of the simplest quantum systems that display the peculiarity of quantum mechanics. Indeed, it is a two-state quantum mechanical system, e.g., an electron in two possible

Manuscript received September 20, 2021; revised December 1, 2021; accepted December 6, 2021. Date of publication December 13, 2021; date of current version January 5, 2022. The work of Daniela Alessandra Zaidenberg was supported by a joint program of the Massachusetts Institute of Technology (MIT) and University of Sannio through the MIT Science and Technology Initiative. This work was supported in part by the European Space Agency Φ-Lab's Quantum Computing for Earth Observation Initiative. *(Corresponding author: Alessandro Sebastianelli.)*

Alessandro Sebastianelli and Silvia Liberata Ullo are with the Engineering Department, University of Sannio, 82100 Benevento, Italy (e-mail: sebastianelli@unisannio.it; ullo@unisannio.it).

Daniela Alessandra Zaidenberg is with the Massachusetts Institute of Technology, Cambridge, MA 02139 USA (e-mail: dzaiden@mit.edu).

Dario Spiller and Bertrand Le Saux are with the European Space Agency, 00044 Frascati, Italy (e-mail: Dario.Spiller@esa.int; bls@ieee.org).

Digital Object Identifier 10.1109/JSTARS.2021.3134785

levels (spin up and spin down) or a single photon in one of the two possible states (vertical and horizontal polarization). While in a classical system, a bit can be in one state or the other, qubit exists in a coherent superposition of both states simultaneously, a property that is fundamental to quantum mechanics. Quantum computers utilize the principles of superposition and entanglement to streamline computation [16]–[18]. For every n qubits, 2^n possible states can be represented. This is an exponential improvement with respect to the classical systems, which can only represent n states for every n bits. Moreover, quantum systems exist in a high-dimensional space, known as a Hilbert space, whose inherent properties lend themselves to a complex linear optimization.

The application of quantum technology for remote sensing has been considered for at least last 20 years. In [19], an active imaging information transmission technology for satellite-borne quantum remote sensing is proposed, providing solutions and technical basis for realizing active imaging technology relying on quantum mechanics principles. Another application discussed in the literature is related to interferometric synthetic aperture radars [20], [21]. In [20], Otgonbaatar and Datcu describe a residue connection problem in the phase unwrapping procedure as quadratic unconstrained binary optimization problem, which is solved by using the D-Wave quantum annealer. The same authors in [21] present a quantum annealer application for subset feature selection and the classification of hyperspectral images.

The research presented in this article focuses on the possibility to use quantum computers to enhance the performances of machine learning (ML) algorithms when applied to land-use and land-cover (LULC) classification, chosen as an EO use case. The results of the multiclass novel QCNN classifier prove the effectiveness of the proposed approach, which is able to achieve better results with standard models of comparable complexity and on-par results with best standard models of the state of the art.

It is worth to highlight that only very few works have addressed the application of quantum machine learning (QML) to remote sensing in the current state of the art. For instance, quantum computers and convolutional neural networks (CNNs) are considered together for accelerating geospatial data processing in [22], where quanvolutional layers [23] are used. These layers contain several quanvolutional filters that transform the input data into different output feature maps by using a number of random quantum circuits, in an analogous way to standard convolutional networks. Quantum-circuit-based neural network classifiers for multispectral land-cover classification have been introduced in preliminary proof-of-concept applications, as presented in [24], and an ensemble of support vector machines running on the D-Wave quantum annealer has been proposed for remote sensing image classification in [25]. In our preliminary work [26], hybrid quantum–classical neural networks for remote sensing applications are discussed, and a proof of concept for binary classification, using multispectral optical data, is reported. Finally, Otgonbaatar and Datcu [27] proposed a binary classifier based on a very deep convolutional network and a 17-qubit quantum circuit.

In this article, different circuit-based hybrid quantum convolutional neural networks (QCNNs) are discussed, and a remote sensing image classification use case is considered, exceeding the simple binary classification presented in [26] and the more complex presented in [27]. Namely, hybrid networks based both on classical and QC will be used, and a comparison of provided performances will be made, when dealing with different quantum circuits applied to classification of remote sensing images.

The main contributions of this work are as follows.

1) QC is applied to land-cover classification on the reference benchmark EuroSAT dataset [28] for optical multispectral images, thus by going further than initial proofs of concept on a few images [24], [25].
2) QCNN multiclass classification is tackled with respect to the simple binary classification already discussed in [26], and better results are obtained through the quantum-based networks with respect to their fully classical counterpart.
3) A comparative and critical analysis is carried out to analyze the performances of different gate-based circuits for hybrid QCNN, showing the advantages of the architecture with entanglement.
4) A structured prediction setting, with coarse-to-fine classification, has been implemented to further challenge the capacities brought by entanglement.

Moreover, it is worth to highlight that each model we proposed has been implemented and designed from scratch. This process also involves the adaptation of the classical and quantum networks to fit the requirements imposed by the used dataset.

It is also worth to mention that this article can represent a useful tool for ML and remote sensing scientists looking at the way quantum circuits and their parameters work when applied to practical EO problems, since it describes the necessary mathematical and physical elements for the understanding of the quantum approach.

The rest of this article is organized as follows. In Section II, an overview of LULC classification in the field of remote sensing is given by highlighting the main issues and difficulties in LULC tasks for remote sensing interpretation. In Section III, the applications of ML in the domain of QC are introduced, and in Section IV, the mathematical and physical background to QC is provided. The proposed methodology and the hybrid QCNNs are presented in Section V, while the results are reported in Section VI. Finally, Section VII concludes this article.

II. LULC Classification Overview

LULC classification using remote sensing imagery has been playing an important role in sustaining, monitoring, and planning the usage of natural resources since years. LULC classification has reached a crucial scope in the management of land use, agricultural sector, forest areas, and biological resources [29], and it has a direct impact on atmosphere, soil erosion, and water, while it is indirectly connected to global environmental problems [30], by helping in delivering up-to-date and large-scale information on surface conditions.

A general overview of supervised object-based land-cover image classification techniques is reported in [31], whereas

a more comprehensive and recent review of challenges and state-of-the-art techniques for LULC classification is provided by Talukdar *et al.* [32].

For years, classical techniques mainly based on pixel or object analysis in terms of reflectance or local texture have been used for LULC classification [33], [34]. Yet, they have shown several issues since they are extremely affected by the data acquisition issues (such as cloud cover and regional fog, adaptation to new sensors) and environmental changes, which make it difficult to design a generic classifier suitable for every object or land class everywhere in the world.

Several new methodologies have been developed by the researchers to address those issues by building on more robust statistical models and, in particular, the well-known deep learning (DL). Two trends have emerged: object-based image analysis (OBIA) or patchwise classification, and dense pixelwise classification.

Generally, patchwise approaches focus on local neighborhoods, which correspond to semantically meaningful objects to build the classifiers. The task to achieve is to give a label to a patch, which corresponds to a small region of a complete aerial or satellite image, as in the popular EuroSAT [35] or BigEarthNet [36] benchmarks. Dedicated OBIA methods can then be applied, which look for relevant objet borders for example, as the DOTA baseline, which is based on a region-based CNN [37].

On the contrary, pixelwise approaches follow the historical remote sensing way of modeling local appearance statistics. In the last decade, the use of fully convolutional networks (FCNs) have proved to be extremely efficient by relying on very large models able to capture the diversity of possible inputs, and, thus, for a large variety of LULC classes: CNNs and random fields [38], multimodal multiscale FCNs [39], and ensemble of CNNs [40].

Finally, among the new techniques adopted to deal with LULC problems, we must include strategies based on capsule networks [41], recurrent networks [42], and graph convolutional networks [43], which have been applied to hyperspectral imagery for instance, and transformers, which has been more recently applied to both patchwise and pixelwise classification [44], [45]. Building on this set of powerful tools, new challenges can now be addressed, which include explainable and interpretable classification [46], weakly supervised classification [47], self-supervised classification, or semisupervised classification [48].

After DL, which has proved to be a relevant tool for improving pre-existing classical models, the beginning of the era of QC has brought new ideas to solve the LULC classification problems, as new opportunities (the amount of data available), but also new issues (large-scale processing, variety of sensors, and very high resolution) have appeared.

III. Quantum Machine Learning

As already underlined before, the research presented in this article focuses on the possibility to demonstrate how the use of quantum computers can help in enhancing the performance of ML algorithms when applied to LULC classification.

In this section, a brief review of the recent results and research open questions concerning QML is first reported. The benefits of QC for ML applications are explained, by highlighting the general advantages of QML and by also presenting some applications. Finally, the open challenges of these approaches and existing systems are discussed.

A. Need for QC

Given the premises of the Introduction section concerning the disruptive potentialities of QC, and the issues discussed in the previous section on the difficulties in LULC tasks for remote sensing interpretation, QML has quickly become a topic of interest for the information science [49]–[52] since the 1990s. As already anticipated, with the continuously increasing volume of data requiring classification-related processing tasks, computers have had to adapt themselves to process these larger and more complex sets of information. This is why quantum solutions are gaining attention and being explored. Moreover, for ML applications, quantum computers may provide an added benefit since they can avoid getting stuck at relative minima in gradient descent, by quantum tunneling through "hills" [53]. Practically, quantum computers are likely to reach a better solution than classical computers. Moreover, QC provides many other benefits for ML, such as fast linear algebra, quantum sampling, quantum optimization, and quantum artificial neural networks [54]. Despite the still unsolved limitations, quantum resources are expected to provide advantages for learning problems.

B. Advantages of QML

As briefly mentioned at the end of the previous subsection, there are several advantages in using the QC applied to ML, and some examples are found in the literature. In [55], for instance, Cong *et al.* introduce and analyze the QCNN as an ML-inspired quantum circuit model and demonstrate its ability to solve important classes of intrinsically quantum many-body problems. They consider two classes of problems, where QC offers some advantages: 1) the quantum phase recognition, which asks whether a given input quantum state belongs to a particular quantum phase of matter, and 2) the quantum error correction (QEC) optimization, where an optimal QEC code is chased, for a given, *a priori* unknown, error model, such as dephasing or potentially correlated depolarization in realistic experimental settings.

Currently, different quantum algorithms that could act as building blocks of ML programs have been developed, sometimes related to hardware and software challenges that are not yet completely solved [50]. Given that ML and AI can play fundamental roles in the quantum domain [52], the main benefits of QML, as already summarized in [56], are the following: 1) improvements in runtime; 2) learning capacity improvements; and 3) learning efficiency improvements.

However, there is not a shared consensus on how and when QML can be advantageous with respect to its classical counterpart on general classes of problems. For instance, in [57], it is shown how the quality and the amount of data can sensibly affect the performance of classical and QML models in such a

way that the quantum advantage is not always guaranteed. With this regard, this article adds an important element of discussion with respect to the state of the art, by demonstrating how QML could help when dealing with real remote sensing images for a classification problem where multiple classes are used.

C. QML Applications

Currently, there are several general methods for implementing quantum circuits into ML models, as it can be found in the literature. For instance, in [58], image classification is performed via a QML, while in [59], a quantum support vector machine is used for Big Data classification. In [23], quanvolutional neural networks are employed to carry out image recognition, and instead, variational quantum circuits for inductive Grover oracularization are presented in [60]. Lithology interpretation from well logs is discussed in [61], and a quantum variational autoencoder is presented in [62]. Quantum neural networks (QNNs) are often presented as hybrid algorithms that leverage quantum nodes throughout the networks [63]–[65]. QNNs develop a network of both quantum and classical nodes with some given activation functions, convolutional connections, and weighted edges. Here, the quantum nodes can be represented by single qubits or clusters of qubits. QNNs can also present a more complexly integrated circuit with entanglement, where correlations between quantum nodes can be exploited to speed up computation.

D. QML Challenges

Trying to create complex quantum networks, which link together layers of quantum nodes, still represents a research challenge. Despite the many possible theoretical applications of quantum computers, there is still significant progress that must be made toward more reliable computation. The QC industry currently finds itself in the NISQ era, where there is a limit to the number of operations that can be performed on a quantum computer before the stored information becomes useless [13]. Currently, these limitations contribute to the difficulties in scaling up quantum computers. However, all the work in progress is not useless since as soon as scaling quantum computers become viable, they will be able to represent exponentially more information than the classical ones. Fortunately, recent events show promising evidence for moving ahead and away from the NISQ era. In particular, by using QCNN models, researchers have been able to create an optimal QEC scheme for a given error mode [55], and moreover, many QC companies are also projecting similar timelines for developing their architecture. Some companies are planning to release error-corrected and fault-tolerant commercial quantum computers by 2025 [66], [67].

IV. Mathematical Background on QC

In this section, the basic notions of QC are introduced. Further information can be retrieved in [17] and [18].

Qubits are the fundamental units of information held in quantum computers. A physical qubit exists in a *superposition* of two states, $|0\rangle$ and $|1\rangle$, as shown in Fig. 1 referring to a hydrogen atom with ground and excited states. The state $|\psi\rangle$ of the qubit describes the probability distribution of the state and is expressed as

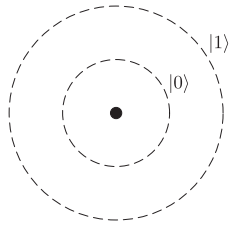

Fig. 1. Qubit modeling as hydrogen atom, with electron ground state $|0\rangle$ and first exited state $|1\rangle$.

$$|\psi\rangle = \alpha|0\rangle + \beta|1\rangle. \tag{1}$$

Quantum measurement is an irreversible operation, in which information is gained about the state of a single qubit, and superposition is lost. Mathematically speaking, in (1), $|\psi\rangle$ can be viewed as a vector in a Hilbert Space (i.e., a vector space equipped with an inner product operation), where

$$|0\rangle = \begin{pmatrix} 1 \\ 0 \end{pmatrix}, \quad |1\rangle = \begin{pmatrix} 0 \\ 1 \end{pmatrix} \tag{2}$$

$\alpha, \beta \in \mathbb{C}$ represent the probability of measuring the states $|0\rangle$ and $|1\rangle$, respectively, with the constraint $|\alpha^2| + |\beta^2| = 1$. For the state $|\psi\rangle = \sqrt{\frac{1}{3}}|0\rangle + \sqrt{\frac{2}{3}}|1\rangle$, the probabilities of measuring $|0\rangle$ and $|1\rangle$ are $\frac{1}{3}$ and $\frac{2}{3}$, respectively. Moreover, the measurement process does irreversibly modify the qubit, so that after the measurement, the qubit can be $|\psi\rangle = |0\rangle$ with probability α^2 and $|\psi\rangle = |1\rangle$ with probability β^2.

When considering a system of two qubits with states $\alpha_0|0\rangle + \alpha_1|1\rangle$ and $\beta_0|0\rangle + \beta_1|1\rangle$, the state evaluated by means of the tensor product is the superposition given by

$$|\psi\rangle = \alpha_0\beta_0|00\rangle + \alpha_0\beta_1|01\rangle + \alpha_1\beta_0|10\rangle + \alpha_1\beta_1|11\rangle \tag{3}$$

where $\alpha_i, \beta_j \in \mathbb{C}$ and $\sum \alpha_i\beta_j = 1$. The state $|00\rangle$, for instance, is given as $|0\rangle \otimes |0\rangle$, where $\otimes$ is the tensor product. It turns out that, in general, you cannot factorize the state in (3) in terms of the original qubits. This phenomenon, known as *entanglement*, has an important consequence in the measurement process. Indeed, considering the *Bell* state

$$|\psi\rangle = \frac{1}{\sqrt{2}}|00\rangle + \frac{1}{\sqrt{2}}|11\rangle \tag{4}$$

if the measurement of the first qubit returns the state $|0\rangle$ (with probability 0.5), then the entangled state collapses to $|00\rangle$. At this point, the second qubit is completely known as it is in the state $|0\rangle$ as well. This result is true even when the two qubits are separated by a very large (theoretically infinite) distance, leading to the violation of the locality principle of classical mechanics. By using the Schmidt decomposition theorem, it can be shown that a quantum system can have different degrees of entanglement [68]. By exploiting superposition and entanglement, quantum computers can perform operations that are difficult to

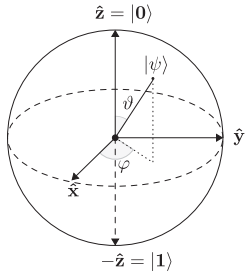

Fig. 2. Bloch sphere representing the probabilistic space in which the quantum state can exist. Gate operations rotate $|\psi\rangle$ about the Bloch sphere, changing the phase and the probability amplitudes of the qubit.

emulate on a large scale with classical computers, cutting down computational time and power to process information.

The qubit state in (1) can be expressed as a function of two angles ϑ and φ, i.e.,

$$|\psi\rangle = \cos\frac{\vartheta}{2}|0\rangle + e^{i\varphi}\sin\frac{\vartheta}{2}|1\rangle \tag{5}$$

and represented as a point sitting on the surface of a unitary 3-D sphere, named the Bloch sphere, as shown in Fig. 2. With this notation, ϑ describes the probability of the qubit to result in $|0\rangle$ or $|1\rangle$ and the angle φ describes the phase the qubit is in.

Quantum gates, denoted by U in the following, are basic quantum circuits operating on a small number of qubits. They are the building blocks of quantum circuits, such as classical logic gates are for conventional digital circuits. Quantum gates are unitary operators, i.e., $U^\dagger U = UU^\dagger = I$, where the symbol $\dagger$ denotes the conjugate transpose, and U is described as a unitary matrix relative to some basis. Important properties are that 1) U preserves the inner product of the Hilbert space and 2) qubit gate operations can also be visualized as rotations of the quantum state vector in the Bloch sphere.

The standard quantum gates used in this article are introduced hereafter.

1) *Hadamard* gate, a single qubit gate described by the matrix

$$H = \frac{1}{\sqrt{2}}\begin{pmatrix}1 & 1\\ 1 & -1\end{pmatrix}. \tag{6}$$

Starting from the single state qubit $|0\rangle$, the Hadamard gate return the superposition of two states, namely the so-called *plus* state $|+\rangle$, i.e.,

$$\begin{aligned} H|0\rangle &= \frac{1}{\sqrt{2}}\begin{pmatrix}1 & 1\\ 1 & -1\end{pmatrix}\begin{pmatrix}1\\0\end{pmatrix} = \frac{1}{\sqrt{2}}\begin{pmatrix}1\\1\end{pmatrix}\\ &= \frac{1}{\sqrt{2}}\begin{pmatrix}1\\0\end{pmatrix} + \frac{1}{\sqrt{2}}\begin{pmatrix}0\\1\end{pmatrix}\\ &= \frac{1}{\sqrt{2}}|0\rangle + \frac{1}{\sqrt{2}}|1\rangle = |+\rangle. \end{aligned} \tag{7}$$

2) *Rotation* gates, $R_x(\theta)$, $R_y(\theta)$, $R_z(\theta)$, i.e., single-qubit gates described by rotation matrices about the $\hat{\mathbf{x}}$, $\hat{\mathbf{y}}$, and $\hat{\mathbf{z}}$ axes of the Bloch sphere, respectively. The gate $R_y(\theta)$, which will be used in the following, takes the form

$$R_y(\theta) = \begin{pmatrix}\cos\frac{\theta}{2} & -\sin\frac{\theta}{2}\\ \sin\frac{\theta}{2} & \cos\frac{\theta}{2}\end{pmatrix}. \tag{8}$$

3) CNOT gate, which is a two-qubit gate described by the matrix

$$U = \begin{pmatrix}1 & 0 & 0 & 0\\ 0 & 1 & 0 & 0\\ 0 & 0 & 0 & 1\\ 0 & 0 & 1 & 0\end{pmatrix} \tag{9}$$

and represented in Fig. 3. When the input are basis states $|0\rangle$ and $|1\rangle$, the CNOT gate transforms the state

$$\alpha_{00}|00\rangle + \alpha_{01}|01\rangle + \alpha_{10}|10\rangle + \alpha_{11}|11\rangle$$

into

$$\alpha_{00}|00\rangle + \alpha_{01}|01\rangle + \alpha_{10}|11\rangle + \alpha_{11}|10\rangle$$

i.e., it flips the second qubit (the target qubit) if and only if the first qubit (the control qubit) is $|1\rangle$.

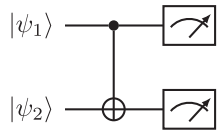

Fig. 3. CNOT gate with two input qubits and measurement output.

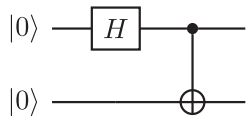

Fig. 4. Quantum circuit to create Bell state.

The combination of Hadamard and CNOT gates is used to create an entangled Bell state, as defined in (4). The corresponding circuit shown in Fig. 4 is the basic building block of the quantum circuits investigated in this article, as it introduces entanglement in the circuit by enhancing the computation performances.

V. Methodology

In this section, a selected number of quantum circuits, investigated as potential quantum layers in the proposed hybrid network, are described. First, the integration of the quantum part into the classical architecture is discussed, by presenting the *"Data Embedding"* operation and showing an example of interface between classical and quantum layers. At the end of the section, the hybrid QCNN is presented, and the model optimization and inference are discussed. Although the quantum circuits presented in the following are standardly used in QC for data processing and they are fundamental units of IBM Qiskit [69], [70], it is worth to highlight that all codes have been realized from scratch by the authors and released open access in a public repository [71].

A. Data Embedding

To create a hybrid QNN, a parameterized quantum circuit is typically used as a hidden layer for the neural network. Yet, with respect to classical network architectures, right in order to integrate the quantum part into the classical architecture, it is critical to realize a higher dimensional quantum representation of classical data in the creation of the hybrid model. In this section, a brief description on how to prepare a quantum state at this end is given.

A feature mapping is first run through a unitary operator applied to a set of N $|0\rangle$ quantum nodes as a method of encoding the classical information in the new N-qubit space. A unitary matrix, needed to encode the information, must be classically derived before applying it to the quantum circuit. Its parameters are determined by the values of the preceding classical nodes at the point of insertion. This operation is referred to as data embedding, where the preceding classical activation is represented through the related amplitude probability of measuring $|1\rangle$ in the quantum state.

Different gate operations can be used to encode a quantum representation of classical information. For instance, Abbas *et al.* [51] show how that can be done by first applying a Hadamard gate to put the qubits in a superposition state and then by applying RZ-gate rotations to the qubits, with angles equivalent to the feature values of preceding inputs. Alternate gate operations can be used to encode a quantum representation of classical information. Yet, the interpretation of the prepared state must be self-consistent, which means to consider the encoding system valid as long as the input operations and the output measurement accurately represent the classical information.

Proceeding the classical encoding, the parameterized quantum circuit is then applied. A parameterized quantum circuit is a quantum circuit, where the rotation angles for each gate are specified by the components of a classical input vector. The outputs from the neural network's previous layer will be collected and used as the inputs for the parameterized circuit. The measurement statistics of the quantum circuit can then be collected and used as inputs for the following hidden layer. As a demonstrative example in Fig. 5, the interface between classical and quantum layers is sketched.

B. Selected Quantum Circuits for Image Classification

Three types of circuits, selected among the possible quantum circuits and to be used in the proposed hybrid QCNN, are presented. Their structure reflects the adopted implementation with four qubits, which represents a more complex architecture with respect to simpler ones where fewer qubits are used [26]. Far from being an exhaustive comparison of all possible quantum configurations, the description of the adopted circuits will allow us to get an insight on how their gates can influence the final results and help speed up certain computational processes. To better understand how the entangled qubits, introduced in Section IV, can affect the classification performance, it is necessary to clarify that the first circuit has no entanglement, whereas entanglement is introduced in the remaining ones through different gate connections.

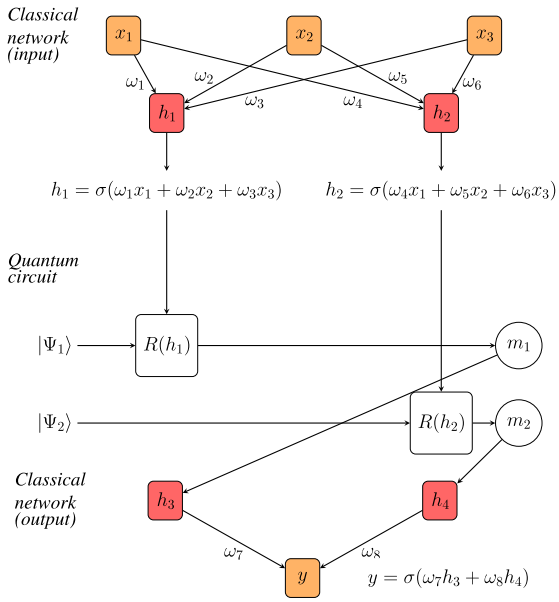

Fig. 5. Interface between classical and quantum layers.

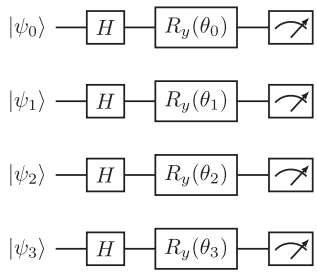

Fig. 6. No entanglement circuit.

1) No Entanglement Circuit: In the simple QCNN presented in [26], there is no entanglement, and classical nodes are merely replaced by a parameter's quantum node [63]. As seen in Fig. 6, the qubits are first placed in superposition through the application of a Hadamard gate.

Next, the quantum nodes undergo R_y gate rotations about the parameters θ. This whole process is ultimately representative of quantum node activation, which simply encodes the sum of the weighted activations from preceding classical nodes that are mapped into the quantum nodes. If only one qubit is considered, the effect of the Hadamard and rotation gates on the qubit $|0\rangle$ is summarized as

$$\begin{aligned} R_y(\theta)H|0\rangle &= \frac{1}{\sqrt{2}}\begin{pmatrix}\cos(\frac{\theta}{2}) & -\sin(\frac{\theta}{2})\\ \sin(\frac{\theta}{2}) & \cos(\frac{\theta}{2})\end{pmatrix}\begin{pmatrix}1 & 1\\ 1 & -1\end{pmatrix}\begin{pmatrix}1\\ 0\end{pmatrix} \\ &\overset{\text{Eq. (7)}}{=} \frac{1}{\sqrt{2}}\begin{pmatrix}\cos(\frac{\theta}{2}) & -\sin(\frac{\theta}{2})\\ \sin(\frac{\theta}{2}) & \cos(\frac{\theta}{2})\end{pmatrix}(|0\rangle + |1\rangle) \\ &= \frac{\cos(\frac{\theta}{2}) + \sin(\frac{\theta}{2})}{\sqrt{2}}|0\rangle + \frac{\cos(\frac{\theta}{2}) - \sin(\frac{\theta}{2})}{\sqrt{2}}|1\rangle. \end{aligned} \tag{10}$$

The overall gate composed of four Hadamard and four rotation gates can be built by using the matrix multiplication for

TABLE I
F1 SCORE + ACCURACY

Model	F1 Score										Accuracy
	Annual Crop	Forest	Herb. Vegetation	Highway	Industrial	Pasture	Perma. Crop	Residential	River	Sea Lake	
Classical v1	0.83	0.91	0.79	0.63	0.90	0.73	0.70	0.92	0.77	0.97	0.83
Classical v2	0.81	0.94	0.76	0.67	0.91	0.83	0.70	0.89	0.73	0.95	0.83
No entanglement circuit	0.83	0.93	0.79	0.00	0.87	0.86	0.65	0.89	0.74	0.96	0.79
Bellman Circuit	0.82	0.89	0.78	0.72	0.94	0.78	0.69	0.94	0.80	0.97	0.84
Real Amplitudes Circuit	**0.90**	**0.98**	**0.89**	**0.86**	**0.96**	**0.92**	**0.84**	**0.97**	**0.87**	**0.98**	**0.92**

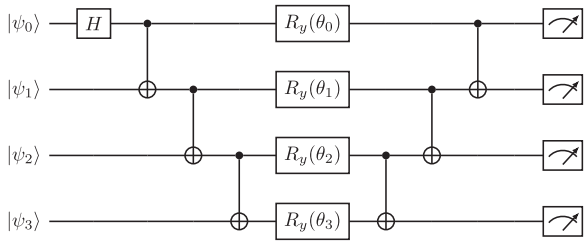

Fig. 7. Bellman circuit.

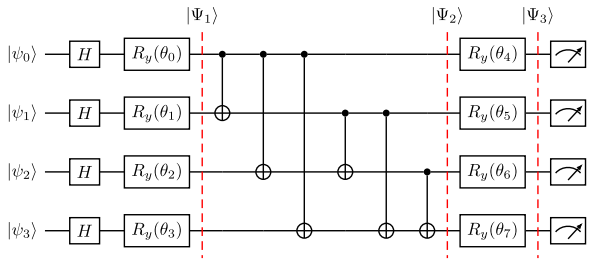

Fig. 8. Real Amplitudes Circuit.

successive gates and the tensor product for parallel gates; hence, the final unitary transformation U is

$$U^* = \bigotimes_{i=0}^{i=3} \left(R_y(\theta_i) \cdot H\right). \tag{11}$$

The entire circuit returns the state

$$|\psi\rangle = U^*(|\psi_0\rangle \otimes |\psi_1\rangle \otimes |\psi_2\rangle \otimes |\psi_3\rangle) \tag{12}$$

which, when considering $|0\rangle$ as inputs, is

$$|\psi\rangle = U^*|0000\rangle. \tag{13}$$

2) Bellman Circuit: The Bellman Circuit shown in Fig. 7 leverages a basic system of entanglement to encode classical information into a quantum space. Here, the speedup may lie in the fact that the quantum states are prepared first through entanglement (by means of the Hadamard and CNOT gates) leading to correlational associations. Following the entanglement process, the parameterization using angular rotations predefined by classical information once more translates the classical information as a quantum activation.

The qubits are first entangled through the application of a Hadamard gate and then sequential CNOT gates. Following this, the qubits are rotated about the y-axis using parameters θ. This is the basis of the activation process. Then, the CNOT application process is reversed, but the superposition is never removed. The benefit of this process seems to lie in the variation of the encoding and rotation process, as it is now not just a projection of the classical information into a quantum space, but rather a transformation of this information that exploits quantum feature space.

Considering the four inputs as $|0\rangle$, before entering into the rotation gates, the state of the four qubits is given as

$$|\psi\rangle = \frac{1}{\sqrt{2}}|0000\rangle + \frac{1}{\sqrt{2}}|1111\rangle. \tag{14}$$

The four rotation gates applied to the entangled state correspond to the application of the gate

$$R_y^{\otimes 4}(\theta_0, \theta_1, \theta_2, \theta_3) = \bigotimes_{i=0}^{i=3} R_y(\theta_i) \tag{15}$$

corresponding to a 16×16 matrix. Finally, the rotated entangled state passes through three more CNOT gates, and then, it is measured. Supposing that the four rotations are identities (i.e., $\theta_i = 0$, $i = 1, \ldots, 4$), the effect of the three CNOT gates is

$$\begin{aligned}
&\tfrac{1}{\sqrt{2}}|0000\rangle + \tfrac{1}{\sqrt{2}}|1111\rangle \xrightarrow{1^{st}\text{ CNOT}} \tfrac{1}{\sqrt{2}}|0000\rangle + \tfrac{1}{\sqrt{2}}|1110\rangle \\
&\tfrac{1}{\sqrt{2}}|0000\rangle + \tfrac{1}{\sqrt{2}}|1110\rangle \xrightarrow{2^{nd}\text{ CNOT}} \tfrac{1}{\sqrt{2}}|0000\rangle + \tfrac{1}{\sqrt{2}}|1100\rangle \\
&\tfrac{1}{\sqrt{2}}|0000\rangle + \tfrac{1}{\sqrt{2}}|1100\rangle \xrightarrow{3^{rd}\text{ CNOT}} \tfrac{1}{\sqrt{2}}|0000\rangle + \tfrac{1}{\sqrt{2}}|1000\rangle.
\end{aligned}$$

3) Real Amplitudes Circuit: As shown in Fig. 8, breaking down the circuit, each qubit passes through a Hadamard gate and then undergoes a gate rotation with parameters θ (this value is derived from the result of the preceding classical node). This is the process by which the classical information is turned into quantum information. Then, the qubits are all mutually entangled using CNOT gates. For instance, considering identity rotations, i.e., $R_y(\theta_i) = I$, $i = 0, \ldots, 3$, the state before the CNOT gates is

$$\begin{aligned}
|\Psi_1\rangle &= \left(\bigotimes_{i=0}^{i=3} H\right)|0000\rangle = \bigotimes_{i=0}^{i=3}(H|0\rangle) \\
&= \left(\frac{1}{\sqrt{2}}\right)^4 \bigotimes_{i=0}^{i=3}(|0\rangle + |1\rangle) \\
&= 0.25(|0000\rangle + |0010\rangle + |0011\rangle + |0001\rangle \\
&\quad + |0100\rangle + |0110\rangle + |0111\rangle + |0101\rangle \\
&\quad + |1000\rangle + |1010\rangle + |1011\rangle + |1001\rangle \\
&\quad + |1100\rangle + |1110\rangle + |1101\rangle + |1111\rangle).
\end{aligned}$$

[1]QNN graphics made with PlotNeuralNet [76].

TABLE II
PRECISION

Model	Precision									
	Annual Crop	Forest	Herb. Vegetation	Highway	Industrial	Pasture	Perma. Crop	Residential	River	Sea Lake
Classical v1	0.78	0.97	0.84	0.75	0.86	0.75	0.60	**0.97**	0.74	**0.99**
Classical v2	0.82	0.90	0.79	0.65	0.88	0.83	0.68	0.86	0.83	0.98
No entanglement circuit	0.78	0.94	0.74	0.00	0.87	0.82	0.62	0.83	0.66	0.95
Bellman Circuit	**0.92**	0.81	0.77	0.69	0.90	0.73	**0.86**	0.92	0.79	**0.99**
Real Amplitudes Circuit	0.91	**0.98**	**0.92**	**0.85**	**0.99**	**0.94**	0.76	0.95	**0.91**	**0.99**

TABLE III
RECALL

Model	Recall									
	Annual Crop	Forest	Herb. Vegetation	Highway	Industrial	Pasture	Perma. Crop	Residential	River	Sea Lake
Classical v1	0.87	0.86	0.75	0.54	0.96	0.71	0.83	0.88	0.81	0.95
Classical v2	0.80	0.97	0.72	0.67	0.94	0.83	0.71	0.93	0.72	0.91
No entanglement circuit	0.87	0.92	0.86	0.00	0.87	0.89	0.68	0.98	**0.85**	**0.98**
Bellman Circuit	0.74	**0.98**	0.78	0.75	**0.97**	0.83	0.57	**0.97**	0.82	0.94
Real Amplitudes Circuit	**0.89**	**0.98**	**0.87**	**0.86**	0.94	**0.91**	**0.93**	**0.99**	0.83	**0.98**

TABLE IV
COARSE CLASSIFICATION REPORT

Cluster	Precision	Recall	F1 Score
Vegetation	0.97	0.99	0.98
Urban	0.99	0.99	0.99
Water Bodies	0.98	0.95	0.97
Accuracy			0.98
Macro Average	0.98	0.98	0.98
Weighted Average	0.98	0.98	0.98

TABLE V
VEGETATION FINE-GRAIN CLASSIFICATION REPORT

Class	Precision	Recall	F1 Score
Annual Crop	0.93	0.94	0.93
Permanent Crop	0.99	0.98	0.98
Pasture	0.92	0.94	0.93
Forest	0.94	0.89	0.91
Herbaceous Vegetation	0.82	0.95	0.93
Accuracy			0.94
Macro Average	0.94	0.94	0.94
Weighted Average	0.94	0.94	0.94

After the CNOT gates, one can easily verify that this example state is unchanged, i.e., $|\Psi_1\rangle = |\Psi_2\rangle$ (but in the general case it varies). Finally, the quantum parameters θ_i, $i = 4, \ldots, 7$, are implemented by means of the final four rotations. By using (15), the final state is

$$|\Psi_3\rangle = R_y^{\otimes 4}|\Psi_2\rangle.$$

During the validation and testing process, the second θ parameters are used as the "quantum weights" mapping to the following classically fully connected layer of the nodes.

C. Hybrid QNN Classifier

Differently from fully quantum AI models, the proposed QCNN classifier is based on recent hybrid QML models, and it consists of the combination of classical ML and quantum layers [53], [72]. This kind of paradigm [73], [74], mostly used in the computer vision domain, in this article has been transferred and adapted to the remote sensing domain. Moreover, it is worth highlighting that the hybrid solutions are the preferred ones in the current stage of QML, mostly due to technology bottlenecks and limitations [26], [27].

Fig. 9 shows the QCNN structure, where the classical part consists of a CNN derived from the LeNet-5 [75], in which both the number of convolutional layers and the input dimension were changed to fit the input image size. Moreover, with respect to the original LeNet-5 design, the proposed model contains only two fully connected layers, stacked before and after the quantum layer. These two layers are used, respectively, for adapting the input size, needed by the quantum layer, and the quantum layer output size to match the number of classes imposed by the chosen dataset. In other words, the purpose of these two classical neural layers is to ensure *data embedding* from the image space to the quantum capacity and to make possible the coexistence of classical and quantum layers in the hybrid structure.

Regarding the quantum part, the quantum layer (blue box labeled as Quantum Circuit in Fig. 9) aims to benefit of the properties of probabilistic QC. This quantum layer is implemented with one of the circuits described in Section V. In the course of this study, several quantum circuits were tested and analyzed to investigate their potential.

For comparison purposes, two versions of the classical counterpart of the proposed QCNN classifier have been implemented and tested. For the classical CNN classifier 1, the quantum circuit has been replaced with a fully connected layer of 16 nodes, based on the quantum circuit output size. For the classical CNN classifier 2, the quantum circuit has been replaced with a multilayer perceptron with fully connected layers of 10, 32, 64, and 256 nodes.

The experimental dataset under consideration is the "EuroSAT: Land Use and Land Cover Classification with Sentinel-2," a dataset of Sentinel-2 satellite images covering 13 spectral bands and consisting out of ten classes with in total 27000 labeled and georeferenced images [35]. The dataset has

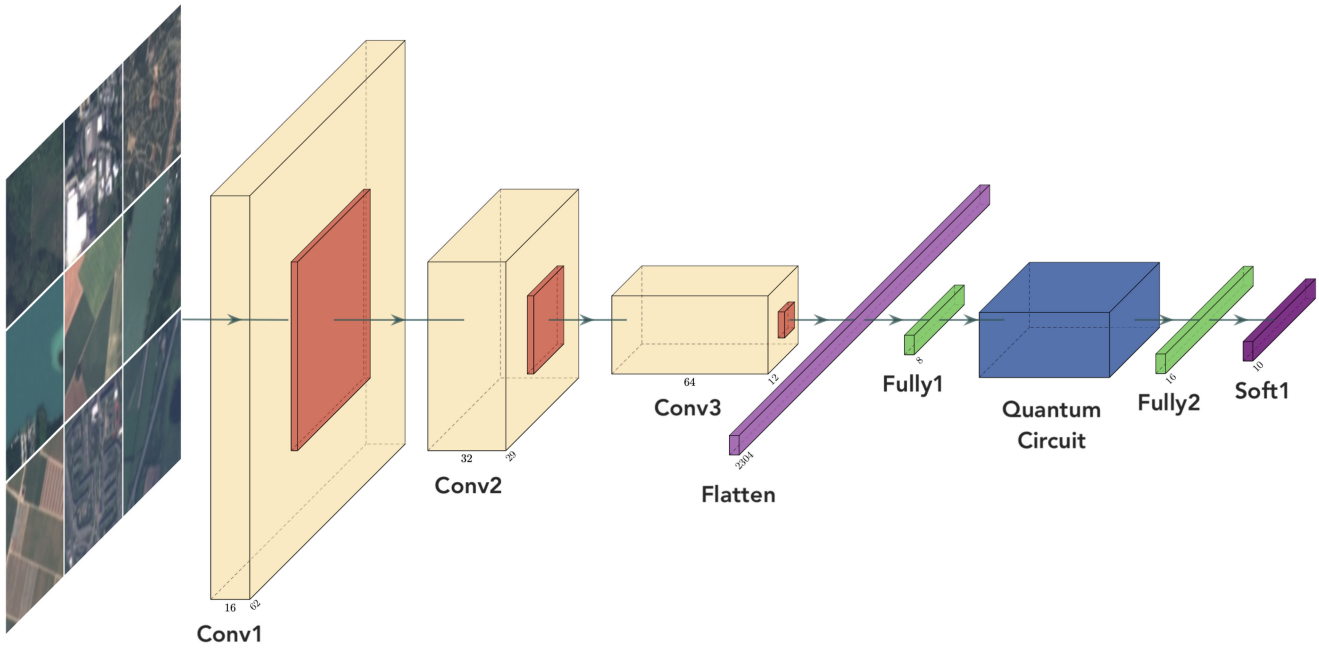

Fig. 9. Proposed hybrid QNN classifier.[1] The network is a modified version of LeNet-5, where the blue box indicates the quantum circuit layer.

been divided in training and validation sets with a 80-20 factor. Sample images of the dataset are shown in Fig. 10.

In the following sections, several experiments have been carried out, such as: 1) experiments on three different quantum circuits; 2) experiments on two classical DL models for comparison with the quantum counterpart; 3) experiments on a coarse quantum classifier and three fine-grain quantum classifiers; and 4) an additional experiment, involving the fine-grain classifier, to create a segmentation map.

As highlighted at the beginning of this section, it is fair to remark that all the proposed models were implemented and designed from scratch. This process also involved the adaptation of the classical and quantum networks to fit the requirements imposed by the dataset used for the experimental analysis. No pretrained weights were used, and the selection of hyperparameters and the loss settings were selected according to the problem requirements.

D. Training and Testing

As stated before, both the training and testing procedures, when possible, have been conducted under the same hypothesis and by using the same settings. All the qubits in Figs. 6–8 are set equal to the state $|0\rangle$.

The models were trained on the Google Colaboratory platform, where each user can count on: 1) a GPU Tesla K80, having 2496 CUDA cores, compute 3.7, 12-G GDDR5 VRAM; 2) a CPU single-core hyper threaded, i.e., (one core, two threads) Xeon Processors @2.3 GHz (No Turbo Boost); 3) 45-MB Cache; 4) 12.6 GB of available RAM; and 5) 320 GB of available disk.

Each QCNN classifier, regardless of the circuit it used, has been trained for 50 epochs, using the Adam optimizer, with a learning rate of 0.0002, and the cross-entropy as loss function. The two classical CNNs have been trained in the same way, but they took ~ 100 epochs to converge.

The training procedure is summarized in Algorithm 1, where the fundamental steps of this process have been reported. The training phase, as happens for any ML model whose training is based on backpropagation algorithms, can be divided into two streams: feedforward and backward. In the first stream, input data pass through both the CNN and the Quantum Circuit, then the overall output is compared with the ground truth, to calculate the error, and through the backward stream, all the model's weights are updated according to the error and its gradient. The testing of the models has been conducted on the validation dataset, according to the procedure summarized in Algorithm 2 for the sake of reproducibility.

VI. Results

A. EuroSAT Dataset Classification

In this section, the results of all the proposed models are presented in the form of confusion matrices and tables with classification reports, showing accuracy, precision, recall, and F1 score, as defined by

$$\text{Accuracy} = \frac{\text{TP} + \text{TN}}{\text{TP} + \text{FP} + \text{FN} + \text{TN}} \tag{16a}$$

$$\text{Precision} = \frac{\text{TP}}{\text{TP} + \text{FP}} \tag{16b}$$

$$\text{Recall} = \frac{\text{TP}}{\text{TP} + \text{FN}} \tag{16c}$$

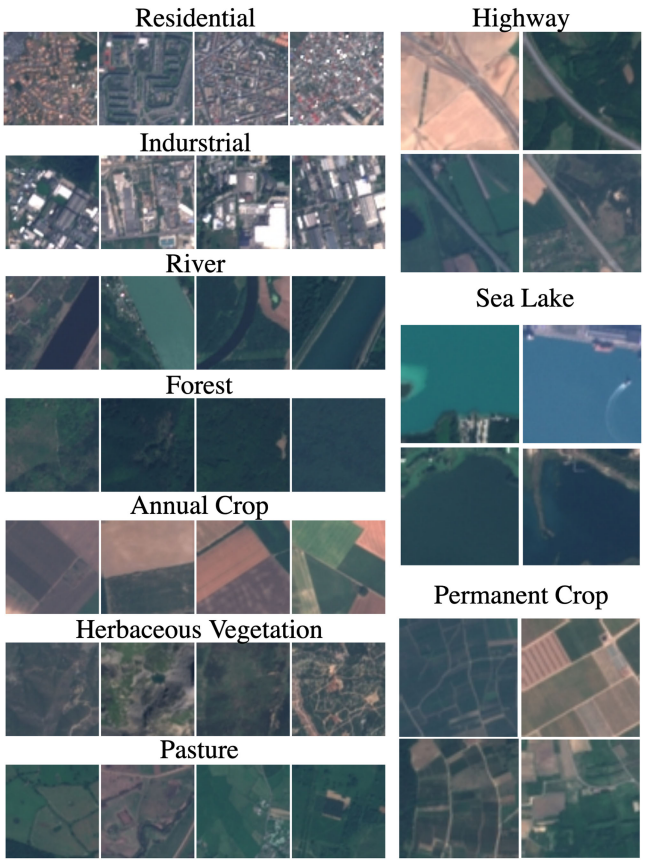

Fig. 10. Sample of the EuroSAT dataset, four images for each class.

$$\text{F1 Score} = 2\,\frac{\text{Recall} \cdot \text{Precision}}{\text{Recall} + \text{Precision}}. \tag{16d}$$

In (16), TP, TN, FP, and FN are the number of true positive cases, true negative cases, false positive cases, and false negative cases, respectively.

In Table I, the F1 scores are reported for each class, together with the overall accuracy, computed on the three proposed quantum classifier and on the two classical counterparts, while in Tables II and III, the precision and recall are reported for each class and for each model mentioned above.

The main evident difference among the quantum-based models is the higher performance when circuits with entanglement are used, thanks to their increased computational capabilities. Both entangled circuits also performed better than the two classical counterparts. Among circuits with entanglement, the Real Amplitudes Circuit reaches the best overall accuracy of 92%, a +10% gain over the second best approach. Delving into details, it has to be underlined that the model using the no entanglement circuit fails to recover the Highway class, one of the classes on which all the classifiers analyzed have found greater difficulties. This result highlights that the choice of the quantum circuit is not only linked to the type of application, but also to the complexity of the data being used. In fact, this circuit has been successfully applied for digit image classification [70], but its effectiveness is poor on more complex remote sensing images.

Algorithm 1: Training of Hybrid Quantum Neural Networks.

```
initializeModel()
for epoch← 0 to epochs by 1 do
    img, groundTruth = loadFromTrainingSet()
    /* Apply CNN                                  */
    featuresMap = applyCNN(img)
    featuresVector = flatten(featuresMap)
    /* Adapt features for Quantum
       Circuit                                    */
    toQuantumCircuit = applyFully1(featuresVector)
    quantumOut =
     applyQuantumCircuit(toQuantumCircuit)
    /* Adapt Quantum Output for
       classification                             */
    classification =
     softmax(applyFullt2(applyQuantumCircuit))
    /* Update Hybird CNN                          */
    error, grad = computeErrorGrad(classification,
     groundTruth)
    updatesCNNWeights(error, grad)
    updatesQuantumWeights(error, grad)
end
```

Algorithm 2: Testing of Hybrid Quantum Neural Networks.

```
model = loadTrainedModel()
for img← to testing set do
    img, groundTruth = loadFromTestingSet()
    append(groundTruths, groundTruth)
    /* Apply Trained Model                        */
    prediction = applyTrainedModel(model, img)
    append(predictions, prediction)
end
/* Get scores                                     */
cm = confusionMatrix(groundTruths, predictions)
accuracy, precision, recall, f1 =
 classificationReport(groundTruths, predictions)
```

In Fig. 11, the confusion matrices for each model are shown. The Real-Amplitudes-Circuit-based QCNN shows the best confusion matrix, with nearly perfect scores on the diagonal. It is able to surpass the performances of all the other quantum-based models and those of the classic models, which all come up against difficulties for specific classes.

B. Coarse-to-Fine Structured Land-Cover Classification

Classification results shown in Section VI-A and especially Table I demonstrate the ability of our hybrid classical–quantum network to perform multiclass EO classification. Even if some-state-of-the-art classical networks achieve better performance (as in [35]), it is worth highlighting that the proposed quantum models are extremely less complex and with very few parameters, as shown in Table IX. Moreover, to further challenge the capacities of our hybrid approach of learning with a limited number of parameters, we propose a structured prediction setting,

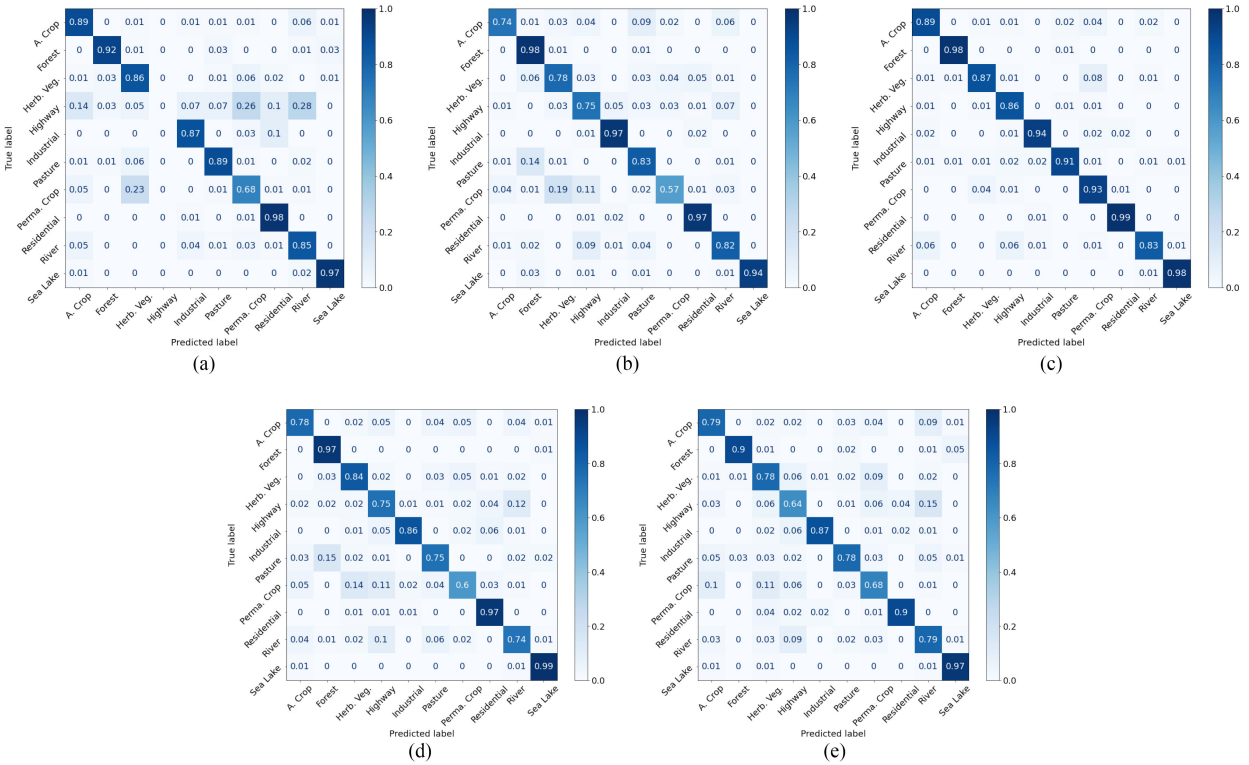

Fig. 11. (a) Confusion matrix for no entanglement circuit. (b) Confusion matrix for Bellman circuit. (c) Confusion matrix for Real Amplitudes Circuit. (d) Confusion matrix for Classical v1. (e) Confusion matrix for Classical v2.

TABLE VI
URBAN FINE-GRAIN CLASSIFICATION REPORT

Class	Precision	Recall	F1 Score
Highway	0.99	0.98	0.99
Residential	0.99	0.99	0.99
Industrial	0.99	0.99	0.99
Accuracy			0.99
Macro Average	0.99	0.99	0.99
Weighted Average	0.99	0.99	0.99

TABLE VII
WATER BODIES FINE-GRAIN CLASSIFICATION REPORT

Class	Precision	Recall	F1 Score
River	0.97	0.99	0.99
Sea Lake	0.99	0.98	0.99
Accuracy			0.99
Macro Average	0.99	0.99	0.99
Weighted Average	0.99	0.99	0.99

TABLE VIII
COARSE-TO-FINE LAND-COVER QUANTUM CLASSIFIER REPORT

Class	Precision	Recall	F1 Score
Annual Crop	0.98	0.93	0.95
Permanent Crop	0.98	0.98	0.98
Pasture	0.93	0.94	0.94
Forest	0.95	0.95	0.95
Herbaceous Vegetation	0.93	0.94	0.94
Highway	0.99	0.99	0.99
Residential	0.99	0.99	0.99
Industrial	0.99	0.99	0.99
River	0.99	0.99	0.99
Sea Lake	0.99	0.99	0.99
Accuracy			0.97
Macro Average	0.97	0.97	0.97

with coarse-to-fine classification, which shows on-par results with the best standard approaches.

Three *difficult* subsets for images of visually similar classes were created. Then, these clusters have been used to train three hybrid QCNNs with the Real Amplitudes Circuit, namely, the fine-grain classifiers. In this way, the four-qubit and the entanglement have been applied within the selected macroclasses and their inherent complexity used to encode details finer than in the overall setup. The proposed clusters are: 1) Vegetation: Annual Crop, Permanent Crop, Pasture, Forest, and Herbaceous Vegetation; 2) Urban: Highway, Industrial, and Residential; and 3) Water Bodies: River and Sea Lake.

The overall structure of the coarse-to-fine land-cover classifier is shown in Fig. 12. A first coarse classifier, based also on the Real Amplitudes Circuit, is trained and applied to divide the data into three macroclasses. Then, based on the coarse classifier output, the corresponding fine-grain classifier is applied to obtain the final classification.

In Table IV, the performances of the coarse classifier only are reported. The proposed model reached an overall accuracy of 98% and an overall F1 score of 98%.

TABLE IX
COMPARISONS WITH STATE-OF-THE-ART AND CLASSICAL METHODS

Model	Overall Accuracy	N. layers	N. parameters
Helber et Al. [35] ResNet-50	0.98	50	25.6M
Helber et Al. [35] GoogleNet	0.98	27	7M
Li et Al. [77] ResNet-18	0.98	18	11M
Sumbul et Al. [36] S-CNN-RGB	0.70	3	23.584
Classical V1	0.82	6	42.338
Classical V2	0.83	7	329.290
No entanglement circuit	0.79	6	42.338 + 4q
Bellman circuit	0.84	6	42.338 + 4q
Real Amplitude circuit	0.92	6	42.338 + 8q
Fine land-cover classifier	0.97	6	42.338 + 8q

The table shows the model used, the overall accuracy, and the number of layers to give an estimate of the complexity. All approaches in the second part of the table are our implementations, described in this article. Other comparisons with classical models can be found in [78].

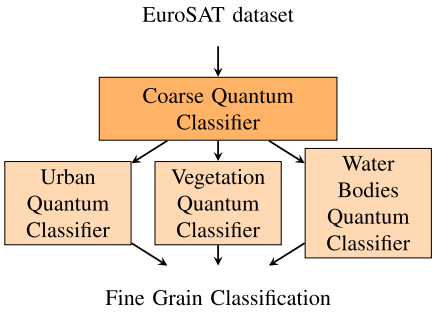

Fig. 12. Coarse-to-fine land-cover classification scheme.

In Table V (respectively, Tables VI and VII), the performances of the fine-grain classifier for the vegetation (respectively, Urban and Water) classes are reported. The proposed models reached overall accuracies of 94–99% and overall F1 scores of 94–99%. This is consistently better if compared with the results for each individual class obtained with the standard classifier (see Table I), meaning that with constant complexity on a slightly reduced dataset, the hybrid QCNN can learn finer details to distinguish similar images.

In Table VIII, the performances of the overall coarse-to-fine-grain classifier are reported. The proposed model reached an overall accuracy of 97% and an overall F1 score of 97%, improving over the standard classifier by +3% and reaching performances on par with Helber *et al.* [35], where the authors reached a 98.57% of overall accuracy, by using a model based on the ResNet-50. It is worth to highlight that the architecture proposed in this article is extremely less complex than the one proposed in [35], since the ResNet-50 is composed of 50 layers, while the proposed one is composed of six layers only: five classical and one quantum. This is an asset for computations in environments with frugal resources. The comparisons are better highlighted in Table IX, where the overall accuracy of classical and quantum models, the size of each model in terms of layers, and the complexity of each model in terms of the number of parameters are reported. Table IX is organized in two branches: the first one containing the results of the state-of-the-art models, while the second one contains the results for both the classical and quantum models proposed in this work.

Finally, graphical results for the Real Amplitudes Quantum Classifier and for the coarse-to-fine land-cover classifier are reported in Tables X and XI, respectively. These tables are structured in order to show correctly and wrongly predicted classes with the idea of underlying the increase of performances introduce with the coarse-to-fine structured land-cover classification.

C. Semantic Segmentation by Patchwise Classification

To further demonstrate the efficiency of the proposed approach, the trained fine-grain quantum classifier has eventually been applied to unseen Sentinel 2 images from the Onera Satellite Change Detection Dataset (OSCD) [79]. In order to run the classifier on these large images, we used a sliding window of 64 $\times$ 64 pixels to match the size of the EuroSAT data, with a step of 32 pixels, leading to a patchwise classification map or semantic map, reproducing the experiment of [80] for comparison to state-of-the-art DL approaches.

Fig. 13 reports the results on one location from OSCD, the city of Beirut. The maps produced by the quantum classifier have been compared with the Wide-ResNet and JEM models presented in [80]. Results are satisfying: the classifier is able to accurately distinguish the urban, vegetation, and water bodies zones along the input image. Moreover, maps are comparable with other state-of-the-art solutions, with even a slight advantage on retrieving residential areas in the very urban area of Beirut.

VII. CONCLUSION

This article investigates the circuit-based hybrid QCNNs for remote sensing image classification. Unlike traditional CNN architectures, the chosen QCNN updates the standard neural network with a quantum layer. The proposed method is applied to the LULC classification tasks, and through a comparative and critical analysis, the performance of different gate-based circuits has been evaluated, and the hybrid QCNN has proven to be effective in terms of multiclass identification and computing efficiency.

Experiments, run on the reference benchmark EuroSAT dataset, have shown that the proposed QCNN worked successfully for the multiclass classification of EO scenes. First, we demonstrated that the architecture with entanglement led to better results by a significant margin with respect to the others. Second, the quantum layer has allowed to reach better results than its classical counterpart. Moreover, all the code and experiments presented in this article have been collected and made available open access in the GitHub page [71]. This material, along with the background on QC given in this article, will hopefully be a useful tool to help the *Geo-science and Remote Sensing* community tackling EO problems with this cutting-edge technology.

Regarding the classical component, which is required for data embedding given the current capacity of NISQ devices, straightforward future work will consist in exploring more powerful networks for data encoding (e.g., compressing the image

TABLE X
EXAMPLE RESULTS OF THE REAL AMPLITUDES QUANTUM CLASSIFIER

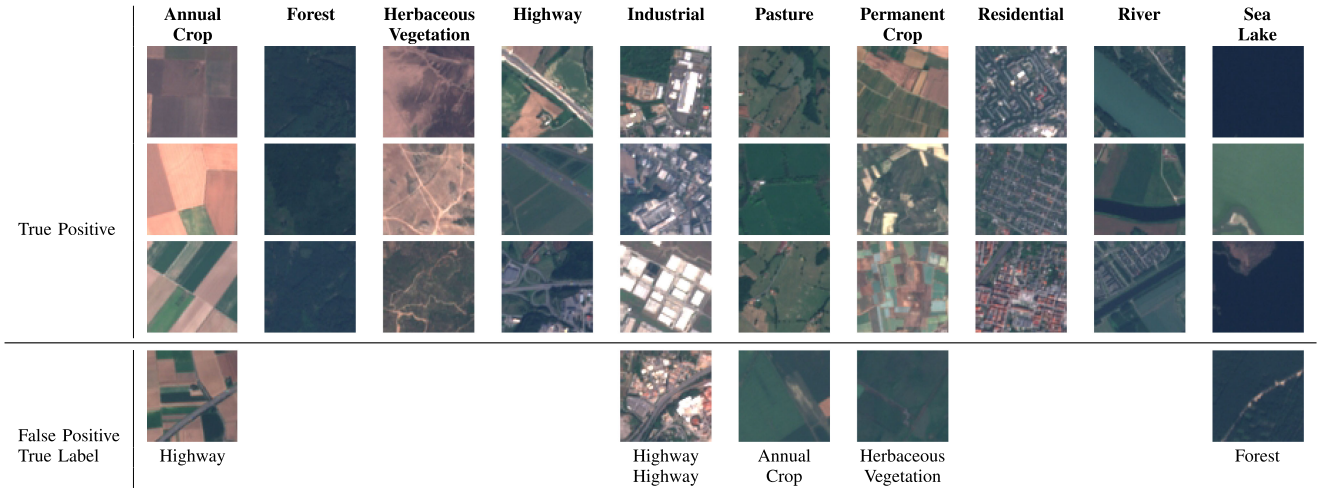

TABLE XI
EXAMPLE RESULTS OF THE COARSE-TO-FINE QUANTUM CLASSIFIER

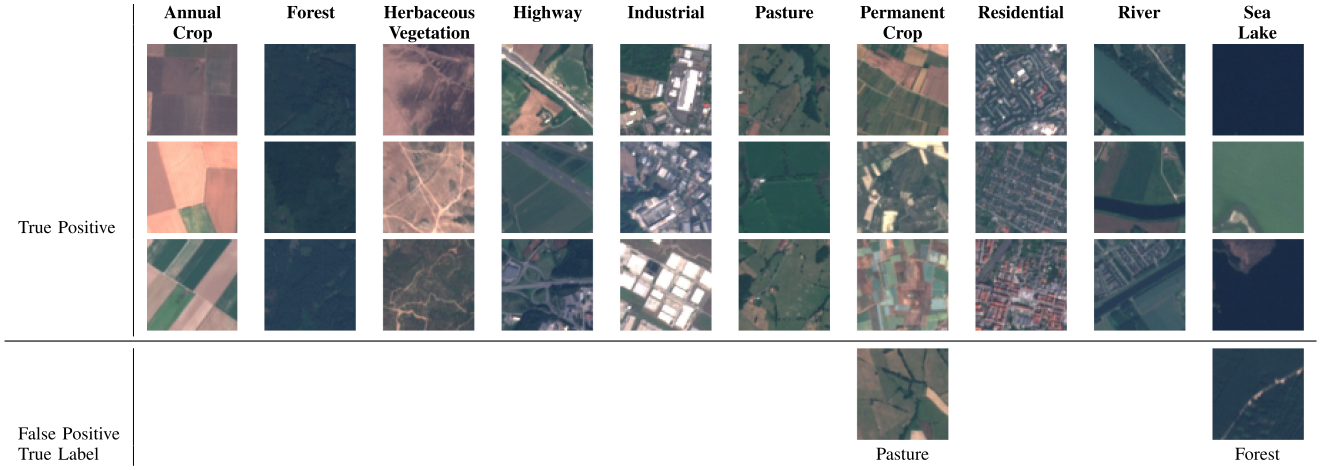

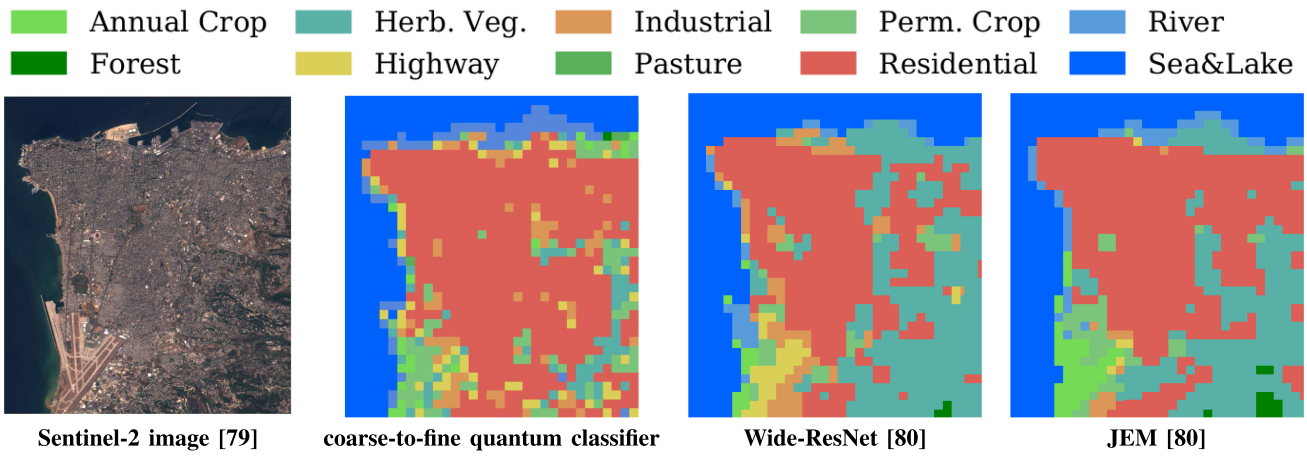

Fig. 13. LULC semantic maps on never-seen OSCD city Beirut compared with the Wide-ResNet and JEM models tested in [80]. (a) Input Image. (b) Coarse-to-fine quantum classifier. (c) Wide-ResNet. (d) JEM.

information in such a way that it may be encoded on the quantum layer). Regarding the quantum component, future work will aim at increasing the proportion of quantum processing in the hybrid approach. Indeed, more complex quantum circuits are expected to enhance the learning power of the model. In particular, quantum convolutions could be examined to incorporate spatial information and invariance in the processing.

More fundamentally, the understanding of the probabilistic mechanisms at work in the quantum layers will represent the key to design better models, develop deep quantum learning, and eventually implement it to many real-life applications.

ACKNOWLEDGMENT

The authors would like to thank Pierre Philippe Mathieu, the Head of Φ-lab explore office and the Ph.D. cosupervisor of Alessandro Sebastianelli, and Giuseppe Borghi, the Head of Φ-lab, for their continual support. The authors would also like to thank Su-Yeong Chang for helpful discussions on mathematics of quantum circuits and Javiera Castillo-Navarro for sharing her expertise for the semantic segmentation experiment.

REFERENCES

[1] S. Rodriguez-Donaire *et al.*, "Earth observation technologies: Low-end-market disruptive innovation," in *Satellites Missions and Technologies for Geosciences*. Rijeka, Croatia: InTech, Jan. 2020.

[2] M. Sudmanns *et al.*, "Big earth data: Disruptive changes in earth observation data management and analysis," *Int. J. Digit. Earth*, vol. 13, no. 7, pp. 832–850, Jul. 2019, doi: 10.1080/17538947.2019.1585976.

[3] G. Denis *et al.*, "Towards disruptions in earth observation? New earth observation systems and markets evolution: Possible scenarios and impacts," *Acta Astronautica*, vol. 137, pp. 415–433, Aug. 2017, doi: 10.1016/J.ACTAASTRO.2017.04.034.

[4] "ESA Earth Online: Working towards AI and earth observation." Accessed: Aug. 24, 2021. [Online]. Available: https://earth.esa.int/web/guest/content/-/article/working-towards-ai-and-earth-observation

[5] P.-P. Mathieu and C. Aubrecht Eds., *Earth Observation Open Science and Innovation*. New York, NY, USA: Springer, 2018, doi: 10.1007/978-3-319-65633-5.

[6] M. P. Del Rosso, A. Sebastianelli, and S. L. Ullo, Eds., *Artificial Intelligence Applied to Satellite-Based Remote Sensing Data for Earth Observation*. London, U.K.: Inst. Eng. Technol., 2021.

[7] M. Riedel, G. Cavallaro, and J. Benediktsson, "Practice and experience in using parallel and scalable machine learning in remote sensing from HPC over cloud to quantum computing," in *Proc. IEEE Int. Geosci. Remote Sens. Symp.*, 2021, pp. 1571–1574.

[8] National Academies of Sciences, Engineering, and Medicine, *Quantum Computing: Progress and Prospects*, E. Grumbling and M. Horowitz, Eds., Washington, DC, USA: National Academies Press, 2019, doi: 10.17226/25196.

[9] F. Arute *et al.*, "Quantum supremacy using a programmable superconducting processor," *Nature*, vol. 574, no. 7779, pp. 505–510, Oct. 2019, doi: 10.1038/s41586-019-1666-5.

[10] C. C. McGeoch, "Theory versus practice in annealing-based quantum computing," *Theor. Comput. Sci.*, vol. 816, pp. 169–183, May 2020, doi: 10.1016/J.TCS.2020.01.024.

[11] H. S. Zhong *et al.*, "Quantum computational advantage using photons," *Science*, vol. 370, no. 6523, pp. 1460–1463, Dec. 2020, doi: 10.1126/SCIENCE.ABE8770.

[12] N. Shettell, W. J. Munro, D. Markham, and K. Nemoto, "Practical limits of error correction for quantum metrology," *New J. Phys.*, vol. 23, no. 4, 2021, Art. no. 043038.

[13] K. Bharti *et al.*, "Noisy intermediate-scale quantum (NISQ) algorithms," 2021, *arXiv:2101.08448*.

[14] A. Peruzzo *et al.*, "A variational eigenvalue solver on a photonic quantum processor," *Nature Commun.*, vol. 5, no. 1, Jul. 2014, Art. no. 4213, doi: 10.1038/ncomms5213.

[15] D. A. Fedorov, B. Peng, N. Govind, and Y. Alexeev, "VQE method: A short survey and recent developments," 2021, *arXiv:2103.08505*.

[16] E. G. Rieffel and W. H. Polak, *Quantum Computing: A Gentle Introduction*. Cambridge, MA, USA: MIT Press, 2011.

[17] P. Kaye, R. Laflamme, and M. Mosca, *An Introduction to Quantum Computing*. New York, NY, USA: Oxford Univ. Press, 2007.

[18] M. A. Nielsen and I. L. Chuang, *Quantum Computation and Quantum Information*. New York, NY, USA: Cambridge Univ. Press, 2011.

[19] S. Bi, "Research on quantum remote sensing science and technology," *Proc. SPIE*, vol. 11128, 2019, pp. 167–186.

[20] S. Otgonbaatar and M. Datcu, "Quantum annealer for network flow minimization in InSAR images," in *Proc. 13th Eur. Conf. Synth. Aperture Radar*, 2021, pp. 1–4.

[21] S. Otgonbaatar and M. Datcu, "A quantum annealer for subset feature selection and the classification of hyperspectral images," *IEEE J. Sel. Topics Appl. Earth Observ. Remote Sens.*, vol. 14, pp. 7057–7065, Jul. 2021, doi: 10.1109/JSTARS.2021.3095377.

[22] M. Henderson, J. Gallina, and M. Brett, "Methods for accelerating geospatial data processing using quantum computers," *Quant. Mach. Intell.*, vol. 3, no. 1, pp. 1–9. 2020.

[23] M. Henderson, S. Shakya, S. Pradhan, and T. Cook, "Quanvolutional neural networks: Powering image recognition with quantum circuits," *Quantum Mach. Intell.*, vol. 2, 2019, Art. no. 2.

[24] P. Gawron and S. Lewinski, "Multi-spectral image classification with quantum neural networks," in *Proc. IEEE Int. Geosci. Remote Sens. Symp.*, 2020, pp. 3513–3516.

[25] G. Cavallaro, D. Willsch, M. Willsch, K. Michielsen, and M. Riedel, "Approaching remote sensing image classification with ensembles of support vector machines on the D-wave quantum annealer," in *Proc. IEEE Int. Geosci. Remote Sens. Symp.*, 2020, pp. 1973–1976, doi: 10.1109/IGARSS39084.2020.9323544.

[26] D. A. Zaidenberg, A. Sebastianelli, D. Spiller, B. L. Saux, and S. L. Ullo, "Advantages and bottlenecks of quantum machine learning for remote sensing," in *Proc. IEEE Int. Geosci. Remote Sens. Symp.*, 2021, pp. 5680–5683.

[27] S. Otgonbaatar and M. Datcu, "Classification of remote sensing images with parameterized quantum gates," *IEEE Geosci. Remote Sens. Lett.*, to be published, doi: 10.1109/LGRS.2021.3108014.

[28] P. Helber, B. Bischke, A. Dengel, and D. Borth, "Introducing EuroSAT: A novel dataset and deep learning benchmark for land use and land cover classification," in *Proc. IEEE Int. Geosci. Remote Sens. Symp.*, 2018, pp. 204–207.

[29] S. Talukdar, P. Singha, Shahfahad, S. Mahato, B. Praveen, and A. Rahman, "Dynamics of ecosystem services (ESS) in response to land use land cover (LU/LC) changes in the lower Gangetic Plain of India," *Ecol. Indicators*, vol. 112, 2020, Art. no. 106121.

[30] Y. H. Tsai, D. Stow, L. An, H. L. Chen, R. Lewison, and L. Shi, "Monitoring land-cover and land-use dynamics in Fanjingshan National Nature Reserve," *Appl. Geography*, vol. 111, 2019, Art. no. 102077.

[31] L. Ma, M. Li, X. Ma, L. Cheng, P. Du, and Y. Liu, "A review of supervised object-based land-cover image classification," *ISPRS J. Photogrammetry Remote Sens.*, vol. 130, pp. 277–293, 2017.

[32] S. Talukdar *et al.*, "Land-use land-cover classification by machine learning classifiers for satellite observations—A review," *Remote Sens.*, vol. 12, no. 7, 2020, Art. no. 1135.

[33] S. Xiaoxia, Z. Jixian, and L. Zhengjun, "A comparison of object-oriented and pixel-based classification approaches using quickbird imagery," pp. 1–3, 2005.

[34] C. Zarro, S. L. Ullo, G. Meoli, and M. Focareta, "Semi-automatic classification of building from low-density Lidar data and worldview-2 images through OBIA technique," in *Proc. IEEE Int. Geosci. Remote Sens. Symp.*, 2020, pp. 992–995.

[35] P. Helber, B. Bischke, A. Dengel, and D. Borth, "EuroSAT: A novel dataset and deep learning benchmark for land use and land cover classification," *IEEE J. Sel. Topics Appl. Earth Observ. Remote Sens.*, vol. 12, no. 7, pp. 2217–2226, Jul. 2019, doi: 10.1109/JSTARS.2019.2918242.

[36] G. Sumbul, M. Charfuelan, B. Demir, and V. Markl, "BigEarthNet: A large-scale benchmark archive for remote sensing image understanding," in *Proc. IEEE Int. Geosci. Remote Sens. Symp.*, 2019, pp. 5901–5904.

[37] G.-S. Xia *et al.*, "DOTA: A large-scale dataset for object detection in aerial images," in *Proc. IEEE Conf. Comput. Vis. Pattern Recognit.*, 2018, pp. 3974–3983.

[38] S. Paisitkriangkrai, J. Sherrah, P. Janney, and A. Van-Den Hengel, "Effective semantic pixel labelling with convolutional networks and conditional random fields," in *Proc. IEEE Conf. Comput. Vis. Pattern Recognit. Workshops*, 2015, pp. 36–43.

[39] N. Audebert, B. Le Saux, and S. Lefèvre, "Semantic segmentation of earth observation data using multimodal and multi-scale deep networks," in *Proc. Asian Conf. Comput. Vis.*, 2016, pp. 180–196.

[40] D. Marmanis, J. D. Wegner, S. Galliani, K. Schindler, M. Datcu, and U. Stilla, "Semantic segmentation of aerial images with an ensemble of CNSS," *ISPRS Ann. Photogrammetry, Remote Sens. Spatial Inf. Sci.*, 2016, vol. 3, pp. 473–480, 2016.
[41] X. Jiang *et al.*, "Hyperspectral image classification with CapsNet and Markov random fields," *IEEE Access*, vol. 8, pp. 191956–191968, 2020.
[42] G. B. Rajendran, U. M. Kumarasamy, C. Zarro, P. B. Divakarachari, and S. L. Ullo, "Land-use and land-cover classification using a human group-based particle swarm optimization algorithm with an LSTM classifier on hybrid pre-processing remote-sensing images," *Remote Sens.*, vol. 12, no. 24, 2020, Art. no. 4135.
[43] D. Hong, L. Gao, J. Yao, B. Zhang, A. Plaza, and J. Chanussot, "Graph convolutional networks for hyperspectral image classification," *IEEE Trans. Geosci. Remote Sens.*, vol. 59, no. 7, pp. 5966–5978, Jul. 2021.
[44] Y. Bazi, L. Bashmal, M. M. A. Rahhal, R. A. Dayil, and N. A. Ajlan, "Vision transformers for remote sensing image classification," *Remote Sens.*, vol. 13, no. 3, 2021, Art. no. 516.
[45] Z. Xu, W. Zhang, T. Zhang, Z. Yang, and J. Li, "Efficient transformer for remote sensing image segmentation," *Remote Sens.*, vol. 13, no. 18, 2021, Art. no. 3585.
[46] D. Tuia, R. Roscher, J. D. Wegner, N. Jacobs, X. Zhu, and G. Camps, "Toward a collective agenda on AI for earth science data analysis," *IEEE Geosci. Remote Sens. Mag.*, vol. 9, no. 2, pp. 88–104, Jun. 2021.
[47] R. Caye Daudt, B. Le Saux, A. Boulch, and Y. Gousseau, "Weakly supervised change detection using guided anisotropic diffusion," *Mach. Learn.*, pp. 1–27, 2021.
[48] J. Castillo-Navarro, B. Le Saux, A. Boulch, N. Audebert, and S. Lefévre, "Semi-supervised semantic segmentation in earth observation: The MiniFrance suite, dataset analysis and multi-task network study," *Mach. Learn.*, pp. 1–36, 2021.
[49] K. N. Sgarbas, "The road to quantum artificial intelligence," 2007, *arXiv:0705.3360*.
[50] J. Biamonte, P. Wittek, N. Pancotti, P. Rebentrost, N. Wiebe, and S. Lloyd, "Quantum machine learning," *Nature*, vol. 549, no. 7671, pp. 195–202, 2017, doi: 10.1038/nature23474.
[51] A. Abbas, D. Sutter, C. Zoufal, A. Lucchi, A. Figalli, and S. Woerner, "The power of quantum neural networks," *Nature Comput. Sci.*, vol. 1, no. 6, pp. 403–409, Jun. 2021, doi: 10.1038/s43588-021-00084-1.
[52] V. Dunjko and H. J. Briegel, "Machine learning & artificial intelligence in the quantum domain: A review of recent progress," *Rep. Prog. Phys.*, vol. 81, no. 7, Jun. 2018, Art. no. 074001, doi: 10.1088/1361-6633/AAB406.
[53] G. Verdon, J. Pye, and M. Broughton, "A universal training algorithm for quantum deep learning," 2018, *arXiv:1806.09729*.
[54] C. Ciliberto *et al.*, "Quantum machine learning: A classical perspective," *Proc. Roy. Soc. A, Math., Phys. Eng. Sci.*, vol. 474, no. 2209, 2018, Art. no. 20170551, doi: 10.1098/RSPA.2017.0551.
[55] I. Cong, S. Choi, and M. D. Lukin, "Quantum convolutional neural networks," *Nature Phys.*, vol. 15, no. 12, pp. 1273–1278, 2019, doi: 10.1038/s41567-019-0648-8.
[56] F. Phillipson, "Quantum machine learning: Benefits and practical examples," in *Proc. Int. Workshop Quantum Software Eng. Programming*, 2020, pp. 51–56.
[57] H.-Y. Huang *et al.*, "Power of data in quantum machine learning," *Nature Commun.*, vol. 12, no. 1, May 2021, Art. no. 2631, doi: 10.1038/s41467-021-22539-9.
[58] H. I. G. Hernández, R. T. Ruiz, and G.-H. Sun, *"Image classification via quantum machine learning*," 2020, *arXiv:2011.02831*.
[59] P. Rebentrost, M. Mohseni, and S. Lloyd, "Quantum support vector machine for big data classification," *Phys. Rev. Lett.*, vol. 113, no. 13, Sep. 2014, Art. no. 130503, doi: 10.1103/physrevlett.113.130503.
[60] A. I. Hasan, "IGO-QNN: Quantum neural network architecture for inductive grover oracularization," 2021, *arXiv:2105.11603*.
[61] N. Liu, T. Huang, J. Gao, Z. Xu, D. Wang, and F. Li, "Quantum-enhanced deep learning-based lithology interpretation from well logs," *IEEE Trans. Geosci. Remote Sens.*, to be published, doi: 10.1109/TGRS.2021.3085340.
[62] A. Khoshaman, W. Vinci, B. Denis, E. Andriyash, H. Sadeghi, and M. H. Amin, "Quantum variational autoencoder," *Quantum Sci. Technol.*, vol. 4, no. 1, Sep. 2018, Art. no. 014001, doi: 10.1088/2058-9565/AADA1F.
[63] K. Beer *et al.*, "Training deep quantum neural networks," *Nature Commun.*, vol. 11, no. 1, 2020, Art. no. 808, doi: 10.1038/s41467-020-14454-2.
[64] J. Liu, K. H. Lim, K. L. Wood, W. Huang, C. Guo, and H.-L. Huang, "Hybrid quantum-classical convolutional neural networks," *Sci. China Phys., Mech. Astron.*, vol. 64, no. 9, pp. 1–8, Aug. 2021, doi: 10.1007/S11433-021-1734-3.
[65] S. Oh, J. Choi, and J. Kim, "A tutorial on quantum convolutional neural networks (QCNN)," in *Proc. IEEE Int. Conf. Inf. Commun. Technol. Converg. (ICTC)*, Sep. 2020, pp. 236–239.
[66] C. Cookson, "PsiQuantum expects commercial quantum computer by 2025." Accessed: Aug. 25. 2021. [Online]. Available: https://www.ft.com/content/a5af3039-abbf-4b25-92e2-c40e5957c8cd
[67] R. Waters, "Goldman Sachs predicts quantum computing 5 years away from use in markets." Accessed: Aug. 25, 2021. [Online]. Available: https://www.ft.com/content/bbff5dfd-caa3-4481-a111-c79f0d38d486
[68] M. A. Nielsen and I. L. Chuang, *Quantum Computation and Quantum Information: 10th Anniversary Edition*. Cambridge, U.K.: Cambridge Univ. Press, 2010, ch. 2.
[69] A. Asfaw *et al.*, "Learn quantum computation using Qiskit," 2020. Accessed: Sep. 10, 2021. [Online]. Available: https://qiskit.org/textbook
[70] C. Liang, "Quantum-deep-learning git-hub page," Accessed: Aug. 25, 2021. [Online]. Available: https://github.com/liangqiyao990210/Quantum-Deep-Learning
[71] D. A. Zaidenberg *et al.*, "QNN 4EO." Accessed: Sep. 10, 2021. [Online]. Available: https://github.com/ESA-PhiLab/QNN4EO
[72] M. Schuld, I. Sinayskiy, and F. Petruccione, "The quest for a quantum neural network," *Quantum Inf. Process.*, vol. 13, no. 11, pp. 2567–2586, Aug. 2014, doi: 10.1007/S11128-014-0809-8.
[73] Y. Liang, W. Peng, Z. J. Zheng, O. Silvéna, and G. Zhao "A hybrid quantum-classical neural network with deep residual learning," *Neural Netw.*, vol. 143, pp. 133–147, Nov. 2021, doi: 10.1016/J.NEUNET.2021.05.028.
[74] A. Mari, T. R. Bromley, J. Izaac, M. Schuld, and N. Killoran, "Transfer learning in hybrid classical-quantum neural networks," *Quantum*, vol. 4, Oct. 2020, Art. no. 340, doi: 10.22331/q-2020-10-09-340.
[75] Y. LeCun *et al.*, "LeNet-5, convolutional neural networks," 2015. Accessed: Sep. 10, 2021. [Online]. Available: http://yann.lecun.com/exdb/lenet
[76] H. Iqbal, "PlotNeuralNet git-hub repository." Accessed: Aug. 24, 2021. [Online]. Available: https://github.com/HarisIqbal88/PlotNeuralNet
[77] J. Li *et al.*, "Deep discriminative representation learning with attention map for scene classification," *Remote Sens.*, vol. 12, no. 9, 2020, Art. no. 1366.
[78] H. Dewangkoro and A. Arymurthy, "Land use and land cover classification using CNN, SVM, and channel squeeze & spatial excitation block," in *Proc. IOP Conf. Ser., Earth Environ. Sci.*, vol. 704, no. 1, 2021, Art. no. 012048.
[79] R. Caye Daudt, B. Le Saux, A. Boulch, and Y. Gousseau, "Urban change detection for multispectral earth observation using convolutional neural networks," in *Proc. IEEE Int. Geosci. Remote Sens. Symp.*, Jul. 2018, pp. 2115–2118.
[80] J. Castillo-Navarro, B. Le Saux, A. Boulch,and S. Lefévre, "Energy-based models in earth observation: From generation to semi-supervised learning," *IEEE Trans. Geosci. Remote Sens.*, to be published, doi: 10.1109/TGRS.2021.3126428.

Alessandro Sebastianelli (Student Member, IEEE) received the Graduate degree (*with laude*) in electronic engineering for automation and telecommunications in 2019 from the University of Sannio, Benevento, Italy, where he is currently working toward the Ph.D. degree.

He was a Visiting Researcher with the Φ-lab, European Space Research Institute, European Space Agency, Frascati, Italy, and still collaborates with the Φ-lab on topics related to deep learning applied to Earth observation. He has coauthored several papers in reputed journals and conferences for the sector of remote sensing. His research interests include remote sensing and satellite data analysis, artificial intelligence techniques for Earth observation, and data fusion.

Mr. Sebastianelli won an ESA OSIP proposal in August 2020 presented with his Ph.D. Supervisor, Prof. Silvia L. Ullo.

Daniela Alessandra Zaidenberg is currently working toward the B.S. degree in physics from the Massachusetts Institute of Technology (MIT), Cambridge, MA, USA.

She is an Undergraduate Researcher with MIT, Cambridge, MA, USA, studying physics and electrical engineering and computer sciences with a focus on quantum information science. She has coauthored a paper entitled "Advantages and bottlenecks of quantum machine learning for remote sensing." She is the President of the Quantum Undergraduate of MIT that serves as a pedagogical platform to teach undergrads about quantum computing, journal club, and guest speakers. She is also a Volunteer Lecturer for qBraid, a startup that teaches high schoolers and first-year undergraduates about quantum computing. She has worked in human–computer interaction engineering, with a focus on user interface design, conductive circuitry, capacitive sensing, and thermistor design.

Dario Spiller (Member, IEEE) received the Ph.D. degree in aereospace engineering from Sapienza Università di Roma, in 2018, with focus on optimal control based on meta-heuristic optimization applied to space problems related to attitude and orbital maneuvers.

He is currently a Postdoctoral Research Fellow working for a joint research project of the Italian Space Agency and the European Space Agency, Frascati, Italy. He is an Aerospace Engineer. He is mainly working on hyperspectral remote sensing and the PRISMA mission with application to wildfire detection and crop-type classification. His current research interests include classification and regression problems applied to remote sensing test cases and solved with machine learning algorithms.

Bertrand Le Saux (Member, IEEE) received the M.S.Eng. degree in signal processing and the M.Sc. degree in signal and image processing from the Instituto Politécnico Nacional de Grenoble, Grenoble, France, in in 1999 and 1999, respectively, the Ph.D. degree in computer science from the University of Versailles/Inria, Versailles, France, in 2003, and the Dr. Habil. degree in machine learning models for scene understanding from the University of Paris-Saclay, Saclay, France, in 2019.

He is currently a Senior Scientist with the European Space Agency/European Space Research Institute F-Lab, Frascati, Italy. His research interests include the visual understanding of the environment by data-driven techniques, including artificial intelligence and (quantum) machine learning with particular focus tackling practical problems that arise in Earth observation, to bring solutions to current environment and population challenges.

Dr. Le Saux is an Associate Editor for *Geoscience and Remote Sensing Letters*. From 2015 to 2017, he was the Co-Chair and from 2017 to 2019, the Chair for the Technical Committee on Image Analysis and Data Fusion of the IEEE Geoscience and Remote Sensing Society.

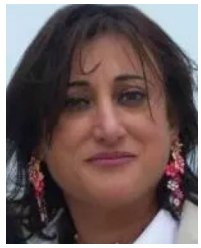

Silvia Liberata Ullo (Senior Member, IEEE) received the Graduate degree (*with Laude*) in electronic engineering from the Faculty of Engineering, University of Naples Federico II, Naples, Italy, in 1989, and the M.Sc. degree from the MIT Sloan Business School, Massachusetts Institute of Technology, Cambridge, MA, USA, in 1992.

Since 2004, she has been a Researcher with the Engineering Department, University of Sannio, Benevento, Italy, where she is a member of the Academic Senate and the Ph.D. Professors' Board. She teaches signal theory and elaboration, telecommunication networks for electronic engineering, and optical and radar remote sensing for the Ph.D. course. She worked in the private and public sectors from 1992 to 2004, before joining the University of Sannio. She has authored more than 80 research papers, coauthored many book chapters, and served as an Editor of two books and many special issues in reputed journals. Her main research interests include signal processing, remote sensing, satellite data analysis, machine learning (ML) and quantum ML, radar systems, sensor networks, and smart grids.

Dr. Ullo is the Industry Liaison for the IEEE Communications Society/IEEE Vehicular Technology Society Joint Italy Chapter. She is the National Referent for the FIDAPA BPW Italy Science and Technology Task Force.